The 15-K neutron structure of saccharide-free concanavalin A

M. P. Blakeley*†‡, A. J. Kalb (Gilboa)§, J. R. Helliwell‡¶, and D. A. A. Myles*¶‖

*European Molecular Biology Laboratory, 6 Rue Jules Horowitz, B.P. 181, 38042 Grenoble Cedex 9, France; †Institut Laue-Langevin, 6 Rue Jules Horowitz, B.P. 156, 38042 Grenoble, France; ‡Department of Chemistry, University of Manchester, Manchester M13 9PL, United Kingdom; and §The Weizmann Institute of Science, 76100 Rehovot, Israel

Edited by Gregory A. Petsko, Brandeis University, Waltham, MA, and approved September 27, 2004 (received for review July 14, 2004)

The positions of the ordered hydrogen isotopes of a protein and its bound solvent can be determined by using neutron crystallography. Furthermore, by collecting neutron data at cryo temperatures, the dynamic disorder within a protein crystal is reduced, which may lead to improved definition of the nuclear density. It has proved possible to cryo-cool very large Con A protein crystals (>1.5 mm^3) suitable for high-resolution neutron and x-ray structure analysis. We can thereby report the neutron crystal structure of the saccharide-free form of Con A and its bound water, including 167 intact D_2O molecules and 60 oxygen atoms at 15 K to 2.5-Å resolution, along with the 1.65-Å x-ray structure of an identical crystal at 100 K. Comparison with the 293-K neutron structure shows that the bound water molecules are better ordered and have lower average *B* factors than those at room temperature. Overall, twice as many bound waters (as D_2O) are identified at 15 K than at 293 K. We note that alteration of bound water orientations occurs between 293 and 15 K; such changes, as illustrated here with this example, could be important more generally in protein crystal structure analysis and ligand design. Methodologically, this successful neutron cryo protein structure refinement opens up categories of neutron protein crystallography, including freeze-trapped structures and cryo to room temperature comparisons.

Water molecules located in both the interior and on the surface of a protein have been shown to play diverse and important roles for the efficient functioning of proteins. Vital information on their hydrogen-bonding interactions can be gained from neutron data. Neutron crystallography can be used to directly assign the positions of hydrogen isotopes in a protein and its bound solvent, which can be done more effectively and at lower resolutions than required with x-rays, thereby providing more information from a diffraction experiment (1). In x-ray protein crystallography, x-rays are scattered in proportion to the number of electrons. Therefore, the ability to locate the hydrogen isotopes of a protein and its bound solvent is only possible if data are available at ultra-high resolution (>1 Å) and critically where the relevant atoms are ordered sufficiently well; an examplar of this approach is the 0.66-Å x-ray study of aldose reductase (2). For neutrons, however, the scattering centers are the atomic nuclei, and each nucleus has a characteristic strong force interaction with a neutron. There is considerably less variation between the elements, and furthermore the interaction can be different for different isotopes of the same element. Hydrogen atoms have a negative neutron scattering length ($b_H = -0.374$), which is of similar magnitude but opposite in sign to C ($b_C = 0.665$), N ($b_N = 0.936$), O ($b_O = 0.580$), and D ($b_D = 0.667$). The practical effect of this sign difference is that hydrogen atoms appear as negative peaks in neutron Fourier maps, in contrast to the majority of atoms, which appear as positive peaks (3) and can help distinguish hydrogen from other atoms. However, at medium resolution (2.0–3.0 Å), negative nuclear density for the hydrogen atoms can simply cancel the positive nuclear density of the atom to which it is attached (4). Water molecules (H_2O) in particular can be difficult to visualize at these resolutions [$(2 \times -0.374) + 0.58$], whereas D_2O heavy water molecules [$(2 \times 0.667) + 0.58$] can be modeled fully as D_2O (5). Therefore, it has been commonplace to exchange H_2O for D_2O by soaking the crystals in a D_2O buffer. Also, a major benefit of exchanging hydrogen for deuterium is that the incoherent scattering from the sample is significantly reduced, since deuterium has a much smaller incoherent scattering cross section than hydrogen.

A number of factors make a neutron protein crystallography experiment more demanding than its x-ray counterpart. The low flux of even the most powerful reactor sources some 10^6 to 10^7 times less intense than the photon fluxes from x-ray synchrotron sources (3) means that data collection times of several weeks to several months are necessary to achieve reasonable counting statistics. In recent years this situation has been considerably improved by developments in instrumentation, detection systems, data processing, and data analysis. In particular, the development of instrumentation designed specifically to harness the power of the Laue technique, and harnessing longer wavelengths to enhance the scattering efficiency, has greatly improved data acquisition times. This development has made feasible many experiments that were previously considered too expensive in terms of the amount of beam time needed. In Laue geometry the sample is illuminated by all available neutrons, thereby maximizing the flux at the sample and stimulating large numbers of reflections simultaneously over all incident wavelengths. A neutron Laue diffractometer (LADI) that incorporates a large-area image plate detector in a cylindrical geometry that fully encircles the protein sample has exploited these advantages to reduce data collection times to just days or even hours (6). A LADI uses a spectral bandpass of the neutron beam that can be tailored by filters to obtain various $\delta\lambda/\lambda$, e.g., 20%. Selection of these filter characteristics (narrow band) are needed to minimize spot–spot overlap when collecting data from large-unit cell systems and also to lower the background count, compared to that of broader band white beams. With the flexibility of this approach it has proved possible to bring 50-kDa neutron protein structure studies in reach (7).

Previously on the LADI, the neutron structure of the D_2O-soaked, saccharide-free form of Con A was determined to 2.4 Å at room temperature (1). Con A is a saccharide-binding protein belonging to the legume lectin family. The monomer of Con A is dominated by an extensive β-sheet arrangement and contains two metal-binding sites (a transition metal-binding site and a Ca^{2+}-binding site), both of which must be occupied for the protein to bind saccharide (8). The Mn^{2+} site has a slightly

This paper was submitted directly (Track II) to the PNAS office.

Abbreviation: LADI, Laue diffractometer.

Data deposition: The atomic coordinates have been deposited in the Protein Data Bank, www.pdb.org (PDB ID code 1XQN).

See Commentary on page 16393.

¶To whom correspondence should be addressed. E-mail: john.helliwell@man.ac.uk or mylesda@ornl.gov.

‖Present address: Oak Ridge National Laboratory, P.O. Box 2008, MS6100, Oak Ridge, TN 37831.

distorted octahedral geometry in which it is coordinated to Asp-10 Oδ1, Asp-19 Oδ1, Glu-8 Oε1, the imidazole Nε of His-24, and two water molecules. The Ca^{2+} site has a pseudooctahedral geometry in which it is coordinated to Asp-10 Oδ1 and Oδ2, Asp-19 Oδ2, Tyr-12 O, Asn-14 Oδ1, and two water molecules. The neutron quasi-Laue study (1) showed the nature of the metal ligand regions of Con A, specifically revealing details of the orientation of the four bound waters' D atoms, which were, as expected, pointing away from the Mn^{2+} and Ca^{2+} ions. The study also allowed the positions and orientations of the bound water D atoms at the saccharide-binding site to be modeled, although the clarity of the nuclear density at the individual waters was poor, i.e., not revealing them singly but rather as a cluster. If the definition of the nuclear density for these water molecules could be improved by lowering the temperature to 15 K so that individual water molecules are observed, more confidence can be placed on the refined D atom positions. Information on the orientation of such waters to the approach of the ligand is important for more complete thermodynamics and modeling studies (9). Therefore, we have now determined the neutron structure at cryo temperature (15 K) on the saccharide-free form of Con A and examined the bound water deuterium atom definition in the neutron maps at low temperature. The overall bound water structure at cryo temperature versus room temperature was studied.

The Mn^{2+}-binding site (*S*1) in Con A has been studied by spectroscopic techniques. Q-band continuous wave EPR studies at room temperature of the Mn^{2+}-binding site in single crystals of Con A were completely consistent with site symmetry implied by the space group, *I*222 (10). However, in recent pulsed EPR and high-field electron nuclear double resonance studies (11–13) the local symmetry at the Mn^{2+} site deviated from the crystal symmetry at low temperatures (4.5 K), but returned to the expected *I*222 symmetry when the crystal was warmed to >205 K. Nevertheless, at all temperatures studied so far by both x-ray and neutron crystallographic techniques (110 K to room temperature) the site symmetry remains *I*222. This finding has led to the hypothesis that there may be two or more Mn^{2+} site structures that average out in the crystallographic experiments at all temperatures, but, on the EPR time scale, averaging occurs only at temperatures >205 K. Possible candidates for such isomerization include low-amplitude motion of the Mn^{2+} ion itself, motion of one (or more) of the ligands, or motion of larger subunits that affects the coordination sphere of the Mn^{2+} ion (13). If, for example, one of the water molecules found as a ligand to the Mn^{2+} ion can rotate about the bisector of the H—O—H bond, the orientation of the unshared-pair electrons may have a profound effect on the electronic properties of the Mn^{2+} ion. Low-temperature neutron diffraction has the potential to examine the orientation of the water molecules by locating the water hydrogen atoms (as deuterium) and thus compare directly with the EPR low-temperature measurements.

Materials and Methods

Crystallization of the Con A Crystals. Very large crystals of Con A, grown by A.J.K.G. by batch dialysis as described (14), were selected for the neutron study. Crystals were grown at room temperature and pH 6.5 from protein solutions in dialysis bags immersed for several weeks in 0.1 M $NaNO_3$, 0.05 M Tris-acetate, 1 mM $MnCl_2$, and 1 mM $CaCl_2$ in D_2O. In previous neutron studies on Con A (1, 4) crystals have been grown from H_2O, and then soaked in D_2O for H/D exchange. In contrast, the crystals used in this experiment were grown directly from D_2O.

Neutron Data Collection, Scaling, and Reduction. Two data sets were collected on the LADI, each of 17 images from two separate crystals; this process was necessitated by awkward scheduling of the data collection run at the research reactor. The two chosen crystals, of dimensions 2.6 × 1.8 × 1.2 mm and 1.8 × 1.3 × 0.7 mm, were soaked in a cryoprotectant mixture of 50:50 (vol/vol) D_2O mother liquor and commercial deuterated 2-methyl-2,4-pentanediol (d-MPD) for 2 h before flash-cooling. The crystals were mounted in fiber loops and flash-cooled by plunging into liquid N_2 (77 K). d-MPD was used as the cryoprotectant to further minimize incoherent scattering from hydrogen atoms. The cryo-cooled crystals were transferred under liquid N_2 and mounted on the cold head of a displex cryostat (set-point 12 K, at sample position 15 K) on the LADI. A restricted narrow bandpass ($\delta\lambda/\lambda = 25\%$) of a long wavelength (range from 2.9 to 3.7 Å) was selected by using a multimirror bandpass filter comprising 40 Si-crystal mirrors, each with 748 alternating 74- to 90-Å-thick Ti and Ni layers. This process was done to reduce background scatter and match the rather large unit-cell axes. Data were collected in 8-degree step intervals about the (phi) rotation axis of the instrument. The exposure time per image was 24 h; 5 min were needed to scan the image plate and 3 min were needed to erase it. An example of the good quality of a typical neutron Laue diffraction image, i.e., in terms of the good spot shape and size, for such a very large cryo-cooled protein crystal can be seen in Fig. 1.

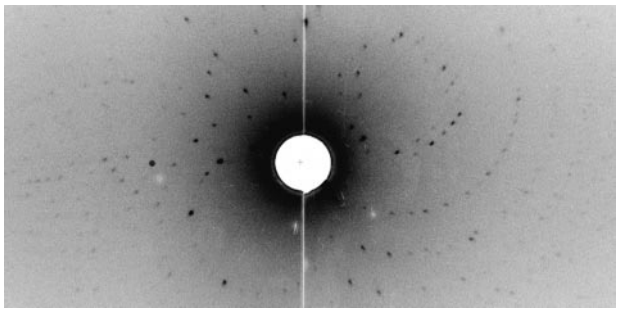

Fig. 1. A neutron Laue diffraction pattern from a large cryo-cooled Con A crystal at 15 K is shown. The volume of the crystal was 5.6 mm^3. [Reproduced with permission from ref. 26 (Copyright 2004, The Royal Society of Chemistry).] A close-up is shown in Fig. 8, which is published as supporting information on the PNAS web site and further illustrates the good diffraction spot shape.

The neutron Laue data were processed by using Daresbury Laboratory (Cheshire, U.K.) software (15, 16) modified for the cylindrical detector geometry and with the polarization correction removed (17). The orientation of each crystal was determined by using the autoindexing routines in the LAUEGEN program (15). The unit cell was refined to: $a = 89.4$ Å, $b = 86.7$ Å, and $c = 62.1$ Å for set 1 and $a = 89.6$ Å, $b = 86.6$ Å, and $c = 62.0$ Å for set 2 (with approximate standard uncertainties on these of 0.3 Å). Integration of each Laue reflection was performed. The program LSCALE (18) was used to derive the wavelength-normalization curve by using the intensities of symmetry-equivalent reflections measured at different wavelengths. No account was made for crystal damage since neutrons do not induce detectable radiation damage and no explicit absorption corrections were applied. The merging *R* factor on *I* was 14.5% for set 1 (9.4% at low to 15.3% at highest resolution) and 14.3% for set 2 (7.0% at low to 15.8% at highest resolution); details of the individual (and combined) data sets are given in Tables 1–3, which are published as supporting information on the PNAS web site, and are reasonably typical of neutron protein data sets, which are usually weaker than x-ray data sets. Although not as good as a single crystal data set, nevertheless the two data sets were sufficiently isomorphous [as a comparison using SCALEIT (19), $R(F) = 26\%$, weighted $R(F) = 15.3\%$] to allow us to combine and merge them together to produce a single data set of 6,462 unique reflections to 2.5-Å resolution with an overall merging *R* factor of 23.5% (14.3% at low to 35.8% at high

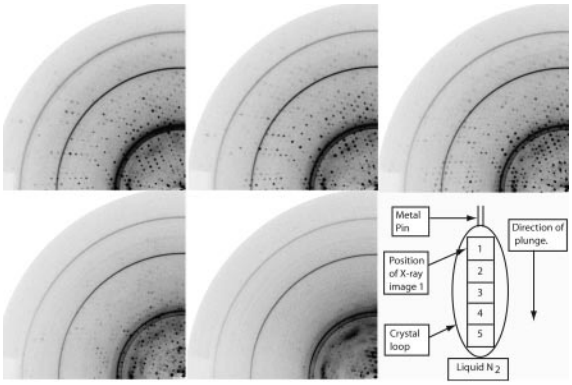

Fig. 2. Quadrants of the five x-ray diffraction patterns produced from the step scan across a large Con A crystal at 100 K are shown. Image numbers 1 (nearest to the pin) to 5 (furthest from the pin) are given. For clarity, shown is a schematic of the crystal in the loop (*Lower Right*), with the positions at which the patterns were taken. *Upper Left* pattern = 1; *Upper Center* pattern = 2; *Upper Right* pattern = 3; *Lower Left* pattern = 4; *Lower Center* pattern = 5.

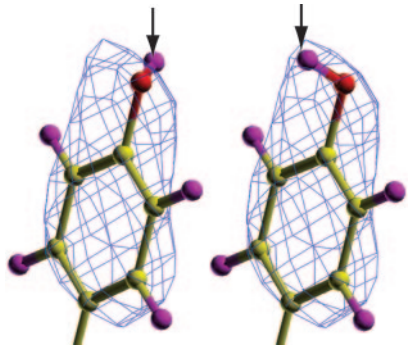

Fig. 3. Before (*Left*) and after (*Right*) refinement of a tyrosine hydroxyl D atom, showing proper positioning of its hydroxyl group, is presented. Figs. 10 and 11, which are published as supporting information on the PNAS web site, further show the quality of the nuclear density with reference to Asn-131 and Phe-197.

resolution) and $<F/\mathrm{sig}(F)>$ = 10.2 (4.3 in outer shell) with completeness 76% (54% in outer shell).

X-Ray Data Collection, Scaling, and Reduction. To provide a good starting model for refinement, we retrieved the crystals used for neutron data collection and determined the atomic positions of an x-ray structure at cryo temperature (100 K) to 1.65 Å on one of them. Since the crystal was large, we performed an x-ray beam step scan along the length of the crystal at five separate positions to determine where a data set should be optimally collected; diffraction patterns from each position are shown in Fig. 2. The step scan showed that the crystalline order varied along the length of the crystal in the plunge direction; ≈60–80% of the crystal was ordered to high resolution. We note that the volume of the crystal closest to the first contact with the liquid nitrogen proved to be the least-ordered region of the crystal. This observation can be rationalized by imagining that the leading surface of the crystal first met boil-off nitrogen gas that was at a higher temperature than that of the cryogenic liquid and the cooling rate was therefore not as good as in the liquid itself. The x-ray diffraction data were collected from an ordered region of the crystal by using a rotating-anode x-ray source fitted with a Mar30cm detector (MAR-Research Hamburg, Germany). The data were processed in DENZO and merged in SCALEPACK (20). The details of the data collection and processing are given in *Supporting Text*, which is published as supporting information on the PNAS web site.

100-K X-Ray Structure Refinement. As the starting structure, the coordinates for the 0.94-Å saccharide-free structure (21) with water molecules removed and the *B* factors reset to 30 $Å^2$ were refined by REFMAC-5 (19) against the 1.65-Å x-ray diffraction data comprising 26,234 unique reflections. ARP_WARP (22) was run to identify water oxygen atom positions. The details are given in *Supporting Text*. The final x-ray model contained 1,809 protein atoms, 3 metal ions (2 Mn^{2+} ions and a Ca^{2+} ion), 8 deuterated 2-methyl-2,4-pentanediol atoms, and 217 water oxygen positions. The second Mn^{2+} ion was unexpected for native Con A although it coincided with a previously determined Cd^{2+} second site (23). The final *R* factor for the 1.65-Å x-ray model was 19.5% with an R_{free} value of 22.0%.

15-K Neutron Structure Refinement. The refined x-ray structure at 1.65 Å was used as the starting model for the neutron refinement by using CNS (24). Hydrogen atoms, as deuteriums where appropriate, were generated for the protein and the bound water oxygen atoms according to standard assignments in CNS. All nonexchangeable hydrogen atoms, i.e., aliphatic hydrogen atoms, were assigned the neutron scattering length for hydrogen ($b_{\mathrm{H}} = -0.374$), whereas all exchangeable hydrogen atoms, i.e., those attached to O or N, were given the neutron scattering length for deuterium ($b_{\mathrm{D}} = 0.667$). The latter includes the approximation that the buried hydrogens in particular, i.e., within the core β-sheet strands, might not have exchanged in practice. At this resolution it is not possible to determine these occupancies directly, which is why this simplifying assumption was made. The first step was a 20-cycle rigid body refinement, using all of the neutron data to 2.5 Å. At this stage the *R* factor was 32.4% and the R_{free} was 34.2%. Next, exchangeable H atom positions (as D atoms) of the protein and bound water were refined (positional and *B* factor refinement) with the rest of the model fixed. The progress of the refinement was checked by manual inspection of the maps. The positions of the exchangeable D atoms of the hydroxyl groups of serine, threonine, and tyrosine residues were seen to refine into the appropriate nuclear density for the model (Fig. 3).

To satisfactorily fit the density for all bound waters, the positions of 210 water oxygen atoms determined by the x-ray structure refinement were required to be shifted. Therefore, positional and *B* factor refinement for the waters, including the water oxygen atoms, was carried out again. This process improved the agreement between the model and the nuclear density. See Fig. 9, which is published as supporting information on the PNAS web site.

To assess whether the individual water sites in the 100-K x-ray and 15-K neutron models corresponded, analysis of the hydrogen-bond interactions was made. If the two waters being compared interacted with the same protein residues/waters then they were deemed to correspond. Of the 217 water oxygen atom positions assigned from the x-ray data, the neutron structure assigned 77 of these as D_2O and 20 as oxygen alone, and 120 had no visible nuclear density. After modeling the position and orientation of the subset of waters that were consistent from the x-ray data, additional waters were added to the model by using the neutron data alone. $F_o - F_c$ maps were calculated and used to identify possible water peaks by using the water-picking procedure in CNS. Water oxygen atoms were assigned if they satisfied certain distance restraints and had positive $F_o - F_c$ map σ values >3.5. Positional and *B* factor refinement of the original water molecules plus the 130 extra added waters was performed, with the rest of the model fixed. $2F_o - F_c$ and $F_o - F_c$ maps showed that of the 130 extra added waters, 90 could be modeled satisfactorily as D_2O, whereas 40 were modeled as oxygen alone. Thus, the

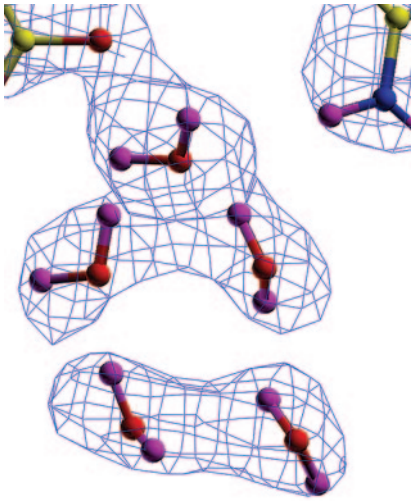

Fig. 4. The 2 $F_o - F_c$ nuclear density at 15 K in blue (at 1.5 rms) for the five water molecules identified at the saccharide-binding site in the neutron model of Con A is shown.

total number of bound waters in the neutron model was 97 + 130 = 227, of which 167 were D_2O and 60 were O only (at this medium resolution there was no attempt made to model O–D).The final *R* factor for the neutron structure was 25.1% and R_{free} was 28.3%.

Results

The Saccharide-Binding Site. The room temperature neutron study (1) had allowed the positions and orientations for three bound waters to be modeled (as D_2O) at the saccharide-binding site. However, the clarity of the nuclear density at these three individual waters had been poor, i.e., not revealing them singly but rather as a cluster. One of the aims of the current study was to improve the definition of the nuclear density for these three water molecules and identify any additional water molecules within the saccharide-binding site. Indeed five water molecules were identified in the 1.65-Å x-ray model at 100 K, and these have been observed in the 2.5-Å neutron model at 15 K also (Fig. 4). However, unlike the x-ray determination in which only the oxygen atoms were revealed, the neutron data have located the positions and orientations of the water D atoms as well.

The *B* factors for the waters have clearly been reduced by collecting the data at lower temperatures. For the five waters at 15 K, their *B* factors are all <5 Å^2, whereas at room temperature, the three waters identified have *B* factors all >20 Å^2.

From analysis of the positions and orientations of the five water molecules in the 15-K model, it has been possible to suggest a hydrogen-bonding network between the water molecules themselves and between key protein residues and the waters. The definition of the H bond used in the analysis is that the distance between proton and proton acceptor is <2.8 Å and the angle (X-D—Y, where X is the proton donor and Y the proton acceptor) is >90°. Fig. 5 gives a schematic of the hydrogen-bonding network in the saccharide-binding site of Con A at 15 K.

Water Structure and *B* Factor Analysis. The final refined 2.5-Å neutron model at 15 K contains 227 water sites. These 227 water sites are all present in the final 2 $F_o - F_c$ nuclear density maps at >1.5 rms. Of these 167 are modeled as D_2O and 60 are modeled as water oxygen atoms alone. The average *B* factor of all of the water atoms is 19.2 Å^2; this value is considerably less than that of the room temperature neutron study at 2.4-Å

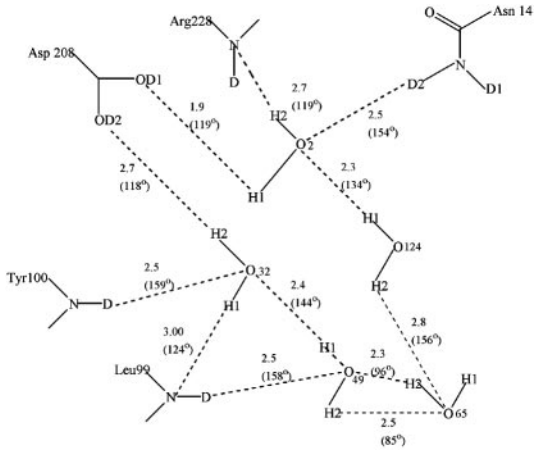

Fig. 5. Schematic of the hydrogen-bonding network in the saccharide-binding site of Con A derived from the neutron data at 15 K is shown.

resolution where the 148 waters identified had an average *B* factor of 43.0 Å^2. Furthermore, the average *B* factor of the 167 D_2O molecules at 15 K is 17.6 Å^2, compared to an average *B* factor of 37.8 Å^2 for the 88 D_2O molecules at room temperature. The average *B* factor for the waters at 15 K that were modeled as oxygen only is 32.2 Å^2. At room temperature, the 60 sites modeled as O or DO had an average *B* factor of 50.6 Å^2. The advantage of collecting the data at cryo temperatures rather than room temperature is that many more waters are observed as D_2O, thus providing a more complete picture of the hydration shells of the protein, which is summarized in Fig. 6. The reduction in dynamic disorder has clearly lowered the *B* factors of the bound water and thereby enhanced the definition of the nuclear density.

An analysis of the position of the bound waters within the monomer was carried out. Of the 227 sites, 16 (13 D_2O, 3 O only) are seen to be completely buried within the protein, whereas 211 (154 D_2O, 57 O only) are surface waters. The buried waters include the four metal-site waters, a water molecule that stabilizes a β-hairpin structure (W16), and a water molecule that stabilizes a β-bulge motif (W22).

The starting 1.65-Å x-ray model was superimposed with the refined 2.5-Å neutron model by using LSQKAB (19), to determine the number of waters that correspond, i.e., are equivalent, between the two structures. Waters were deemed to be equivalent if, after superposition of the two sets of coordinates, the water oxygen atoms agreed to within 1 Å. Of the 227 water

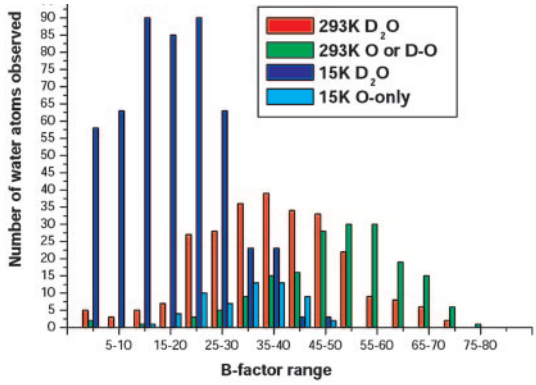

Fig. 6. Plot of the number of water atoms observed that have *B* factors within a given range, at two different temperatures (15 and 293 K) with the *B* values taken from the two neutron structures is shown.

oxygen positions determined by neutron crystallography, 44 (37 as D_2O and 7 as O only) were within 1 Å of the 217 waters in the 1.65-Å x-ray model. The average *B* factor of these 44 waters in the 2.5-Å neutron structure at 15 K was 19.8 Å^2 (average *B* factor for 37 D_2O = 19.0 Å^2, average *B* factor for 7 O-only = 32.5 Å^2). The corresponding average *B* factor in the 1.65-Å x-ray model was 25.3 Å^2.

Of the 16 buried waters in the final refined neutron model at 15 K, 9 matched the positions of the water oxygen atoms in the 1.65-Å x-ray starting model. Of the 211 surface waters in the 15-K neutron structure, 35 matched the positions of the water oxygen atoms in the 1.65-Å x-ray structure. This finding illustrates that a greater percentage of the buried waters agrees with the starting model than the surface waters (56.3% buried agree and 16.6% surface agree) as would be expected because of the increased mobility of surface waters that make fewer interactions with the protein.

The Manganese Site. At the manganese site water molecules were found to be conserved in not only all Con A crystal structures but also all legume lectin crystal structures in general. One would perhaps expect these waters to be in well defined orientations and positions in the neutron structure at 15 K. However, from analysis of the $2F_o - F_c$ and $F_o - F_c$ nuclear density maps at 15 K, one of the two Mn^{2+} site water molecules displayed poor nuclear density and its orientation could not be defined accurately. The disorder of this specific Mn^{2+} site water is illustrated by its *B* value, which is >45 Å^2, whereas the other water coordinated to the Mn^{2+} ion displays strong positive nuclear density and a low *B* factor of 11.3 Å^2. Comparison of the *B* factors of the Mn^{2+} site waters at 15 K with those for the Mn^{2+} site waters at room temperature reveals that the same water site at each temperature has the highest *B* factor. However, at room temperature the Mn^{2+} site water *B* factors are both <35 Å^2. Furthermore, at room temperature the waters appear to be better ordered as they display stronger positive nuclear density.

The definition of the nuclear density at 15 K for the bound waters in general appears to have been greatly improved relative to the room temperature data. This observation is illustrated by the average *B* values for all of the waters at each temperature (19.2 Å^2 at 15 K and 43.0 Å^2 at 293 K) and more specifically, by the improved definition of the saccharide-binding site waters at 15 K. However, this improved definition does not occur at the Mn^{2+} site. The EPR results (11–13) show that while at room temperature there is only one type of Mn^{2+} site, and at low temperatures (4.5–205 K) two types of Mn^{2+} site are distinguished that are chemically inequivalent. It has been suggested that the two types of Mn^{2+} sites observed in the low-temperature EPR studies are possibly caused by the motion of one (or more) of the ligands (13). We have observed disorder at the Mn^{2+} site for one of the water molecules found as a ligand to the Mn^{2+} ion. This finding is in contrast to the room temperature neutron data, in which the positions and orientations of both waters were well defined. At the manganese itself the 15-K nuclear density is perhaps weaker than the room temperature case (1); however, the nuclear scattering length of manganese is small and negative, being almost identical to hydrogen, and so it is difficult to make a quantitative occupancy comparison between the 15- and 293-K results on that specific detail. Nevertheless, the weaker Mn^{2+} density and the disorder of one of the bound waters at the Mn^{2+} site at 15 K in the large cryo-cooled single crystals of Con A is consistent with the results from EPR experiments. We note, however, that the 1.65-Å x-ray structure at 100 K and the 0.94-Å x-ray structure at 110 K (21) do not show disorder at the Mn^{2+} site, which contrasts with the EPR results that already give that indication at 205 K. There is then an inconsistency between the EPR and x-ray cryo crystallography results at these intermediate temperatures.

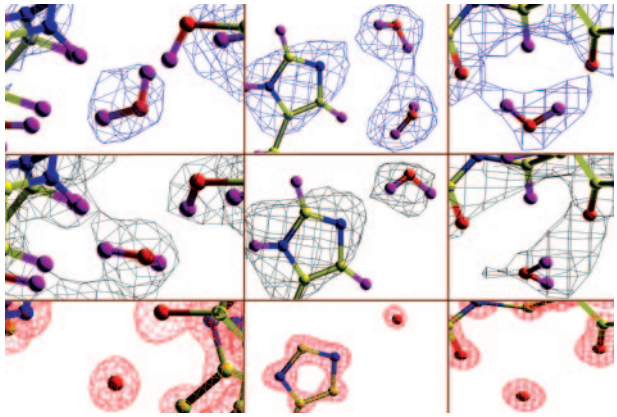

Fig. 7. Comparison of three of the 22 conserved bound water sites studied under the various conditions labeled is shown. (*Left*) W1. (*Center*) W6, but note one extra D_2O position at 15 K. (*Right*) W75. (*Top*) $2F_o - F_c$ nuclear density at 15 K (at 2 rms, in blue). (*Middle*) $2F_o - F_c$ nuclear density at 293 K (at 2 rms, in black). (*Bottom*) $2F_o - F_c$ x-ray density at 110 K (at 3 rms, in red).

Conserved Waters in an Ensemble of Con A Structures. Further comparisons of the water structure of the 15-K neutron model were made against the 2.4-Å neutron model at 293 K (1), the 1.8-Å x-ray model at 293 K (Protein Data Bank ID code 1QNY) (1), and the 0.94-Å x-ray model at 110 K (21). Only 22 water sites (19 as D_2O and 3 as O only) were found to be conserved, i.e., agreed within 1 Å, in all of the Con A structures tested. The average *B* factor of these 22 waters in the 2.5-Å neutron structure at 15 K was 22.1 Å^2 (average *B* factor for 19 D_2O = 21.3 Å^2, average *B* factor for 3 O only = 36.2 Å^2). The average *B* factor of these 22 conserved waters at 293 K was 35.0 Å^2 (average *B* factor for 18 D_2O = 32.7 Å^2, average *B* factor for 4 O only or DO = 45.2 Å^2).

These conserved water sites were examined to discover where they are situated and what interactions they make with their surroundings. In Fig. 7, three of these conserved water sites are shown for the two neutron structures at 15 and 293 K (1) and the ultra-high-resolution x-ray structure at 110 K (21).

For certain sites, the orientation of the water molecules in the neutron structures at 15 and 293 K differs, perhaps suggesting different hydrogen-bonding interactions (Fig. 7 *Left* and *Right*), whereas in other sites the orientation of the water molecules at 15 and 293 K is very similar, in that reasonable hydrogen-bonding interactions (angles and distances) with the same protein residues are made (Fig. 7 *Center*). Changes in the orientation of water molecules between crystal structures at room and cryo temperatures may have important consequences in general for protein crystal structure analysis and ligand design.

Discussion

Because of the inherent low flux of even the most powerful neutron reactor sources, it is necessary to use large crystals with volumes of at least 1 mm^3 to perform high-resolution neutron protein diffraction studies. It was previously thought to have not been possible to successfully cryo-cool crystals of this size. Crystals of Con A considered large for x-ray crystallography have been successfully cryo-cooled previously; the volumes of the crystals used were 0.16 and 0.11 mm^3 (25). We have shown that it is possible to successfully cryo-cool very large Con A protein crystals with volumes of 5.6 and 1.6 mm^3 and to collect neutron data sets at 15 K to 2.5-Å resolution. Thus, the work represents a case study of what is possible for cryo neutron protein crystallography. Furthermore, the generality of being able to cryo-cool very large crystals (>1 mm^3) and study them by neutron protein crystallography is also known to be viable

since 15 K lysozyme (F. Meilleur and D.A.A.M., unpublished data) and rubredoxin (R. Bau, M.P.B., and D.A.A.M., unpublished work) structural studies have been done to 1.7 Å with the LADI instrument at the Institut Laue Langevin in Grenoble; the respective crystal sample volumes in these two cases were ≈4 and 1.4 mm^3.

The 15-K neutron ConA structure has been compared to the 293-K neutron structure (1). Twice as many waters were assigned as D_2O at 15 K than at 293 K, reflecting lower average *B* factors at 15 K than at room temperature. Waters that are conserved at both temperatures are those that are well ordered, have low *B* factors, and display strong positive nuclear density. These waters exhibit small average shifts (≈0.2 Å) in water oxygen atom positions between the 1.65- and 0.94-Å x-ray structures (21) and the 2.5-Å 15-K and 2.4-Å 293-K neutron structures (1). Larger average shifts (≈1 Å) are observed for those waters that have high *B* factors and weaker nuclear density. This finding suggests that, at this resolution, X plus N refinement strategies are appropriate for those water atoms that are identified as conserved between the ensemble of available x-ray structures. In general, though, for future neutron structure refinements to reduce bias from the starting model, we suggest it is better to remove water O atoms identified from the x-ray structure and identify water molecules by using the neutron data alone.

The definition of D_2O water molecules at the saccharide-binding site is greatly improved at 15 K relative to 293 K. Whereas at 293 K, where the waters were identified as a cluster, at 15 K the waters were resolved, allowing the D atom positions to be placed with confidence. This result has allowed a hydrogen-bonding network to be proposed between key amino acid residues in the saccharide-binding site and the conserved water molecules. However, and in contrast to the general improvement in D_2O order, increased disorder was observed at the Mn^{2+} site at 15 K compared to the room temperature data. This observation may correlate with current results from EPR experiments in which the local symmetry at the Mn^{2+} site deviates from the crystal symmetry at low temperatures of 4.5–205 K (11–13). This result was not supported by the 1.65-Å x-ray structure, in the sense that at 100 K good oxygen electron density was observed for both waters.

Overall, neutron crystallography has been shown to be ideally suited to identifying the positions of the hydrogen isotopes of a protein and its bound solvent. Furthermore by collecting the data at cryo temperatures rather than room temperature the definition of the nuclear density has been enhanced. This process has led to more water molecule positions being identified and moreover to greater confidence in the assigned D atom positions.

Analysis of the neutron structure has revealed a wealth of information about the protein and its hydration shells. This information can be integrated into more complete molecular modeling and dynamics calculations in the future. However, as a caution, we note that alteration of bound water orientations occurs between 293 and 15 K; such changes, as illustrated here with this example, could be important more generally in protein crystal structure analysis and ligand design. Methodologically, this neutron cryo protein structure refinement opens up categories of neutron protein crystallography such as cryo to room temperature comparisons and freeze-trapping structural studies.

J.R.H. received research grant support from the Biotechnology and Biological Sciences Research Council and The Wellcome Trust. M.P.B. received Ph.D. studentship support from the Engineering and Physical Sciences Research Council and the Institut Laue Langevin. J.R.H. was awarded neutron beam time on the LADI by the Institut Laue Langevin.

1. Habash, J., Raftery, J., Nuttall, R., Price, H. J., Wilkinson, C., Kalb (Gilboa), A. J. & Helliwell, J. R. (2000) *Acta Crystallogr. D* **56,** 541–550.
2. Howard, E. I., Sanishvili, R., Cachau, R. E., Mitschler, A., Chevrier, B., Barth, P., Lamour, V., Van Zandt, M., Sibley, E., Bon, C., *et al*. (2004) *Proteins* **55,** 792–804.
3. Tsyba, I. & Bau, R. (2002) *Chemtracts-Inorg. Chem.* **15,** 233–257.
4. Habash, J., Raftery, J., Weisgerber, S., Cassetta, A., Lehmann, M. S., Hoghoj, P., Wilkinson, C., Campbell, J. W. & Helliwell, J. R. (1997) *J. Chem. Soc. Faraday Trans.* **93,** 4313–4317.
5. Korszun, Z. R. (1997) *Methods Enzymol.* **276,** 218–232.
6. Myles, D. A. A., Bon, C., Langan, P., Cipriani, F., Castagna, J. C., Lehmann, M. S. & Wilkinson, C. (1998) *Physica B* **241–243,** 1122–1130.
7. Kalb (Gilboa), A. J., Myles, D. A. A., Habash, J., Raftery, J. & Helliwell, J. R. (2001) *J. Appl. Crystallogr.* **34,** 454–457.
8. Kalb (Gilboa), A. J. & Helliwell, J. R. (2001) in *Handbook of Metalloproteins*, eds. Messerschmidt, A., Huber, R., Poulos, T. & Weghardt, K. (Wiley, New York), pp. 963–972.
9. Bradbrook, G. M., Gleichmann, T., Harrop, S. J., Habash, J., Raftery, J., Kalb (Gilboa), A. J., Yariv, J., Hillier, I. H. & Helliwell, J. R. (1998) *J. Chem. Soc. Faraday Trans.* **94,** 1603–1611.
10. Meirovitch, E., Luz, Z. & Kalb (Gilboa), A. J. (1974). *J. Am. Chem. Soc.* **96,** 7538–7542.
11. Manikandan, P., Carmieli, R., Shane, T., Kalb (Gilboa), A. J. & Goldfarb, D. (2000) *J. Am. Chem. Soc.* **122,** 3488–3494.
12. Carmieli, R., Manikandan, P., Kalb (Gilboa), A. J. & Goldfarb, D. (2001). *J. Am. Chem. Soc.* **123,** 8378–8386.
13. Carmieli, R., Manikandan, P., Epel, B., Kalb (Gilboa), A. J., Schnegg, A., Savitsky, A., Möbius, K. & Goldfarb, D. (2003) *Biochemistry* **42,** 7863–7870.
14. Greer, J., Kaufman, H. & Kalb (Gilboa), A. J. (1970) *J. Mol. Biol.* **48,** 365–366.
15. Campbell, J. W. (1995) *J. Appl. Crystallogr.* **28,** 228–236.
16. Helliwell, J. R., Habash, J., Cruickshank, D. W., Harding, M. M., Greenhough, T. J., Campbell, J. W., Clifton, I. J., Elser, M., Machin, P. A., Papiz, M. Z. & Zurch, S. (1989) *J. Appl. Crystallogr.* **22,** 483–497.
17. Campbell, J. W., Hao, Q., Harding, M. M., Nguti N. D. & Wilkinson, C. (1998) *J. Appl. Crystallogr.* **31,** 496–502.
18. Arzt, S., Campbell, J. W., Harding, M. M., Hao, Q. & Helliwell, J. R. (1999) *J. Appl. Crystallogr.* **32,** 554–562.
19. Collaborative Computational Project No. 4 (1994) *Acta Crystallogr. D* **50,** 760–763.
20. Otwinowski, Z. & Minor, W. (1997) *Methods Enzymol.* **276,** 307–326.
21. Deacon, A., Gleichmann, T., Kalb (Gilboa), A. J., Price, H., Raftery, J., Bradbrook, G. M., Yariv, J. & Helliwell, J. R. (1997) *J. Chem. Soc. Faraday Trans.* **93,** 4305–4312.
22. Lamzin, V. S. & Wilson, K. S. (1993) *Acta Crystallogr. D* **49,** 129–143.
23. Naismith, J. H., Habash, J., Harrop, S. J., Helliwell, J. R., Hunter, W. N., Wan, T. C. M., Weisgerber, S., Kalb (Gilboa), A. J. & Yariv, J. (1993) *Acta Crystallogr. D* **49,** 561–571.
24. Brunger, A. T., Adams, P. D., Clore, G. M., Delano, W. L., Gros, P. & Grosse-Kunstleve, R. W. (1998) *Acta Crystallogr. D* **54,** 905–921.
25. Parkin, S., Rupp, B. & Hope, H. (1996) *Acta Crystallogr. D* **52,** 1161–1168.
26. Blakeley, M., Cianci, M., Helliwell, J. R. & Rizkallah, P. J. (2004) *Chem. Soc. Rev.* **33,** 548–557.